HYDROACOUSTIC PROPAGATION AND REFLECTION LOSS USING EXPLOSIONS FOUND IN THE INDIAN OCEAN

Jeffrey A. Hanson, Colin L. Reasoner, and J. Roger Bowman

Science Applications International Corporation

Sponsored by Army Space and Missile Defense Command

Contract No. W9113M-05-C-0138

ABSTRACT

We investigate propagation and reflection loss using hydroacoustic waves from explosion sources in the Indian Ocean recorded at the International Monitoring System's (IMS) hydrophone stations. We developed a discovery procedure that searches the automatic processing results from the International Data Centre (IDC) for signals that match explosive characteristics. Potential candidate explosions are confirmed by examination of the raw waveform data. Using this procedure, we have identified hundreds of explosions throughout the Indian Ocean Basin. The instigators of the explosions are not known, but the locations and characteristics of the explosions lend themselves to likely candidates. These include military exercises, construction, geophysical exploration, and local fishing practices.

We examined hydroacoustic data covering a 6-year period and identified 305 separate explosions. Of these, 25 were recorded at three hydrophone triads – Cape Leeuwin, Australia (H01W), Crozet Island (H04N) and Diego Garcia (H08S) – 79 were recorded at two triads – H04N and H08S – and 201 were recorded at a single triad. In addition, we have observed many airgun surveys, but they are not of interest here due to their local nature. We are able to locate explosions observed at three or two triads using direct arrivals. In some cases, we can locate explosions recorded at a single triad using observed reflections. Absolute arrival times can be estimated to less than 2 seconds, and relative times for closely spaced explosions can often be estimated to within a few samples (4 to 12 milliseconds). Back-azimuth uncertainty estimates range from a few tenths of a degree to several degrees depending on the frequency content of the signal and noise conditions at the triad.

The explosions are distributed in three general locations: the Arabian Sea off northwestern India, the Bay of Bengal, and along the islands of western Indonesia. The explosions in the Arabian Sea and the Bay of Bengal are likely of military origin, while the western Indonesian explosions are more likely from blast fishing. The Arabian Sea explosions occur near a test firing range off shore from Dwarka, India. The Indonesian explosions occur in clusters that correspond to the islands ranging from Simeulue Island in Aceh Province to the northwest tip of Java.

Received signals have energy distributed in frequency starting at 2 to 10 Hz and continuing up to the Nyquist frequency (125 Hz). Peak received levels from the explosions range from 105 to 150 dB rel. 1 μPa. Basic attenuation corrections indicate the yield sizes range from less than one to tens of kilograms. Bubble pulse estimates place a trade-off constraint on source size and depth. The bubble pulse delay time estimates range from 0.1 to 0.5 seconds. The explosions along Indonesia have bubble pulses clustered near 0.2 seconds suggesting that the explosions have similar sizes and depths. Bubble pulse estimates for the same explosion measured at different triads (H04N and H08S) agree to within a few milliseconds.

The explosions are located so that paths to different stations intersect different bathymetry. Most have direct deep water paths to at least one of the hydrophone triads. Attenuation estimates can be made by comparing amplitudes between stations. Relative amplitudes between triads for closely spaced explosions are stable (to within 3 dB) and demonstrate the robustness of attenuation estimates. Attenuation is observed to vary for paths that intersect specific bathymetric features, many of which do not reach the Sound Fixing and Ranging (SOFAR) channel axis. This is particularly evident for paths crossing near the Afanasiy-Nikitin Seamount south of Sri Lanka. Small changes in path (within 100 km) are observed to cause attenuation differences of as much as 20 dB.

OBJECTIVES

This project is designed to improve discrimination of underwater seismic events and improve location of hydroacoustic sources in or just above the water column. This is accomplished by analyzing hydroacoustic data from a multitude of explosion sources to assess high-frequency (>30-50 Hz) signal loss of hydroacoustic energy propagating in the SOFAR channel, from reflections off coastlines, and interaction with bathymetric obstacles along path. We use variations in the observed residual amplitudes to identify important environmental factors that influence high-frequency transmission loss. This allows for better prediction of the reflected wave field and better understanding of the robustness of explosion-characteristic measures from reflected or highly attenuated signals.

RESEARCH ACCOMPLISHED

Data Set of In-Water Explosions

We have discovered 438 explosion signals from 305 distinct in-water explosion sources detonated by other parties in the Indian Ocean and recorded on hydrophone stations of the International Monitoring System (IMS) (Figure 1, Table 1). To identify candidate explosions, we examined results of our automatic processing of Indian Ocean hydrophone stations for the period September 2004 to March 2005 (Hanson et al., 2007). We also examined automatic processing results by the IDC for the period November 2001 through May 2007. The IDC processed data separately from each of the triad hydrophones, whereas our processing treated the triads as arrays. Array processing allowed identification of signals with lower signal-to-noise ratio (SNR), due to array gain, and the estimation of arrival azimuth and slowness.

To find previously unknown in-water explosions, we developed search criteria based on our previous experiences studying long-range propagation of signals produced by small in-water explosions (e.g., Reasoner et al., 2005; Hanson et al., 2001; Brumbaugh and LeBras, 1998). These criteria exploit signal features routinely measured in our own automatic processing of transient hydroacoustic signals (Hanson and Bowman, 2006) or by automatic processing results from the IDC (see e.g., Hanson et al., 2001). The criteria included significant peaks in the estimated cepstrum, broadband energy content (significant energy to at least 80 Hz), short signal durations, and phase velocities consistent with horizontally propagating waves.

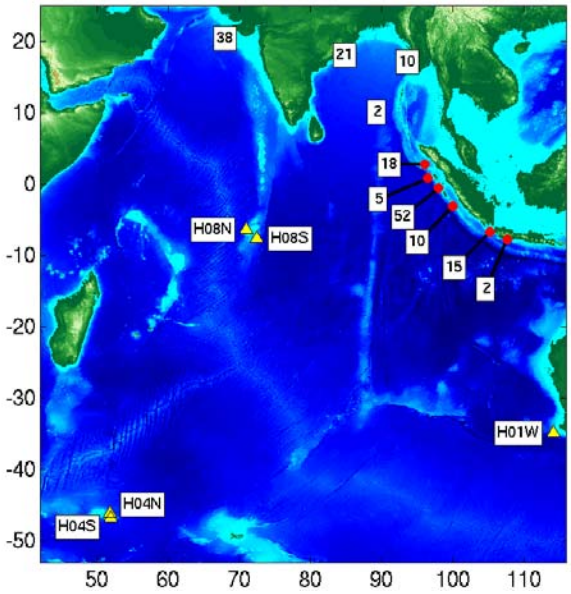

Figure 1. Locations of explosions (numbered squares) recorded at one or more IMS hydrophones (yellow triangles). Numbers indicate sets of explosions in close proximity to one-another.

We conducted an intensive search for in-water explosions in two parts. The first, more comprehensive, search covered a seven-month period of data that spanned from September 2004 through March 2005. These data were processed in-house using the algorithms described in Hanson and Bowman (2006). Signals matching our criteria were examined regardless of peak energy level. The second part of our search covered a six-year period from 2001 to 2007. For this search, we used the automatic processing results from the IDC and further constrained the search criteria to find only larger explosions with a peak received level > 140 dB rel. 1 μPa.

Our search criteria admit some ice events, shallow earthquakes and other unidentified transient signals. Signals from all candidate explosion signals were examined to confirm or refute explosion characteristics. Figure 2 shows spectrograms for three arrivals confirmed as explosions, owing to their high frequency content, scalloped spectra, and short durations. Because the explosions are generally low yield, they are often only detected at one hydrophone

triad by automatic processing. However, more detailed examination of data at other triads, assuming likely source areas, enabled us to find arrivals from the same explosions at multiple stations. In addition, reflected energy is observable for many explosions (Figure 2). We are able to locate many of the explosions based on the multiple arrivals.

Of the 305 explosions we discovered, 25 were recorded at three or more hydrophone triads, 79 were recorded at two triads (H04N and H08S), and 201 were recorded by a single triad. Explosion signals are observed most commonly at Crozet Island North (H04N) and Diego Garcia South (H08S). In addition to the explosions in Table 1, we observed many airgun surveys, but did not investigate them because their signals are generally recorded only by a single, nearby hydrophone triad and are not useful for studying long-range transmission loss. The 305 explosions found in this study dramatically increase the number of known in-water explosions in the Indian Ocean from the 17 explosions detonated on a 2003 traverse from Cape Town to Cocos-Keeling Island (Blackman et al., 2003) and two explosions in 2004 in the Bay of Bengal (Graeber and Firbas, 2005; Spiliopoulos and Jepsen, 2005; Reasoner et al., 2005; Bowman et al., 2005).

Table 1. Explosion arrivals in the Indian Ocean basin

Hydrophone Triad	Number
Cape Leeuwin (H01W)	60
Crozet Island North (H04N)	156
Crozet Island South (H04S)	4
Diego Garcia North (H08N)	42
Diego Garcia South (H08S)	176
Total	438

The explosions in the Indian Ocean basin are distributed in three general locations: the Arabian Sea off northwestern India, the Bay of Bengal, and along the islands of western Indonesia. Figure 1 shows the number of explosions observed in each source area. Explosions offshore of Indonesia are often observed at two or three triads. In contrast, because of signal blockage, explosions offshore of northwestern India are observed by a single triad, H08N, and offshore of Myanmar, only by H08S. Locations for some of these explosions are estimated using back-azimuths and differential arrival times of direct and reflected signals (Hanson and Bowman, 2006). The 38 explosions shown in the Arabian Sea offshore of Dwarka, India are those for which H08N arrivals had valid estimated back-azimuths.

The instigators of the explosions are not known, but the locations and characteristics of the explosions lend themselves to likely candidates. These include local fishing practices (particularly off Indonesia), military exercises (e.g., off India), construction and demolition, and geophysical exploration.

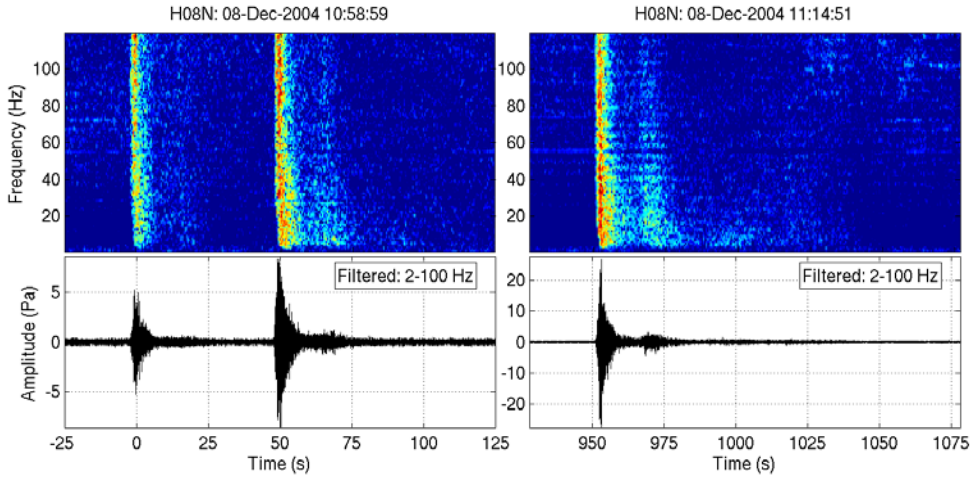

Figure 2. (Left) Spectrogram and waveform of two explosions recorded at Diego Garcia North (H08N). The direct arrivals are broadband signals with frequencies extending from 2 Hz to greater than 100 Hz and are followed by lower amplitude, lower frequency reflected arrivals. (Right) Spectrogram and waveform of an explosion recorded at H08N. The direct arrival and first reflected arrival show clear scalloping from the bubble pulse.

Characterization of Explosions

Explosion signals have energy distributed in frequency starting at 2 to 10 Hz and continuing up to the Nyquist frequency (125 Hz). Peak received levels from the explosions range from 105 to 150 dB rel. 1 µPa. Basic attenuation corrections indicate the yield sizes range from less than one kilogram to tens of kilograms. The explosion signals are concentrated during the daylight hours in the Indian Ocean (Figure 3). This is consistent with our interpretation that these events are man-made explosions.

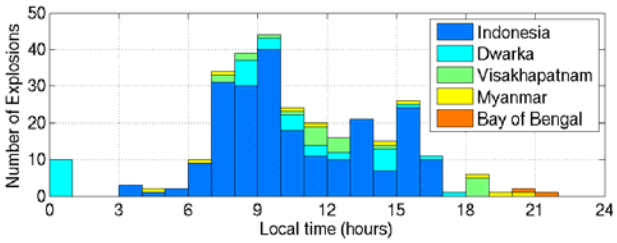

Figure 3. Time of day distribution of explosions color coded by location.

We initially estimated the locations of 102 Indonesian explosions using the measured arrival times and back-azimuths with a standard location algorithm that used the IDC's 2D, seasonal, travel-time tables. Although two arrival time estimates and two back-azimuth estimates are technically enough to uniquely locate events, the uncertainties in back-azimuth—a few tenths of a degree to several degrees depending on the frequency content of the signal and the noise conditions at the triad—projected over thousands of kilometers provide little constraint on locations. However, absolute arrival times can generally be estimated to within 2 s or less. Therefore, we used arrival times as the main data constraint and back-azimuth estimates to confirm associations.

Figure 4 shows how the different data constrain locations. The back azimuths are consistent with locations along Sumatra and Java, but do not put tight constraints on actual locations as seen in Figure 4a, which shows locations based on projected back-azimuth crossing points. Although the arrival time differences between two stations can be measured precisely and the model errors are likely small, a two station time difference does not constrain the location to a point but instead to a continuous curve such that the travel time difference between the two stations remains constant. Because there is no closed form solution on an ellipsoid, we determined these curves by iterative search. In Figure 4b, curves using the arrival time differences between H08S and H04N are shown for each explosion as they intersect Indonesia. The lines overlie one another such that the 102 explosions fall into tight clusters. The uncertainties from measurement error are no wider than the plotted lines. Different assumptions in travel time model can shift the curves by tens of kilometers, but all in the same direction. Although most explosions have only two observations, 23 explosions were observed at H01W in addition to H04N and H08S. These explosions can be located accurately (Figure 4c) and lie just off the coast of the western islands. Since we suspect that the explosions are used for fishing, it is reasonable to expect that the explosions are not far from the islands. Thus, the intersection of the two-station, time-difference curves with the coast is likely close to the actual location. To stabilize our final locations we chose to use the intersection with the 500 meter depth contour—intersections with shallower bathymetry contours are more ambiguous because of their high curvature. Since the bathymetry in the area is steep, the 500 meter contour is only 10 to 20 km from the coast, and thus our locations are likely only slightly biased to the west. Figure 4d shows our final explosion locations.

The explosions occur in clusters that correspond to the islands ranging from Simeulue Island in Aceh Province to western Java (Figure 4d). The events collect into six main groups (labeled A-F), but within each group there are several smaller clusters. Groups A through D appear associated to the islands off western Sumatra and roughly correspond with Simeulue, Nias, Batu and Mentawi Islands, respectively. There is a gap in the explosions between 3˚30'S and 6˚30'S which corresponds to a gap in the western islands with the exception of the lightly populated Enggano Island. If explosions have also been detonated offshore of Sumatra itself, then their signals have been blocked by the bathymetric ridge that extends south of the offshore islands. The explosions in Group E are near Panaitan island in the Ujung Kulon National Park, a world-renowned surf break, and Group F occurs off the coast of West Java Province.

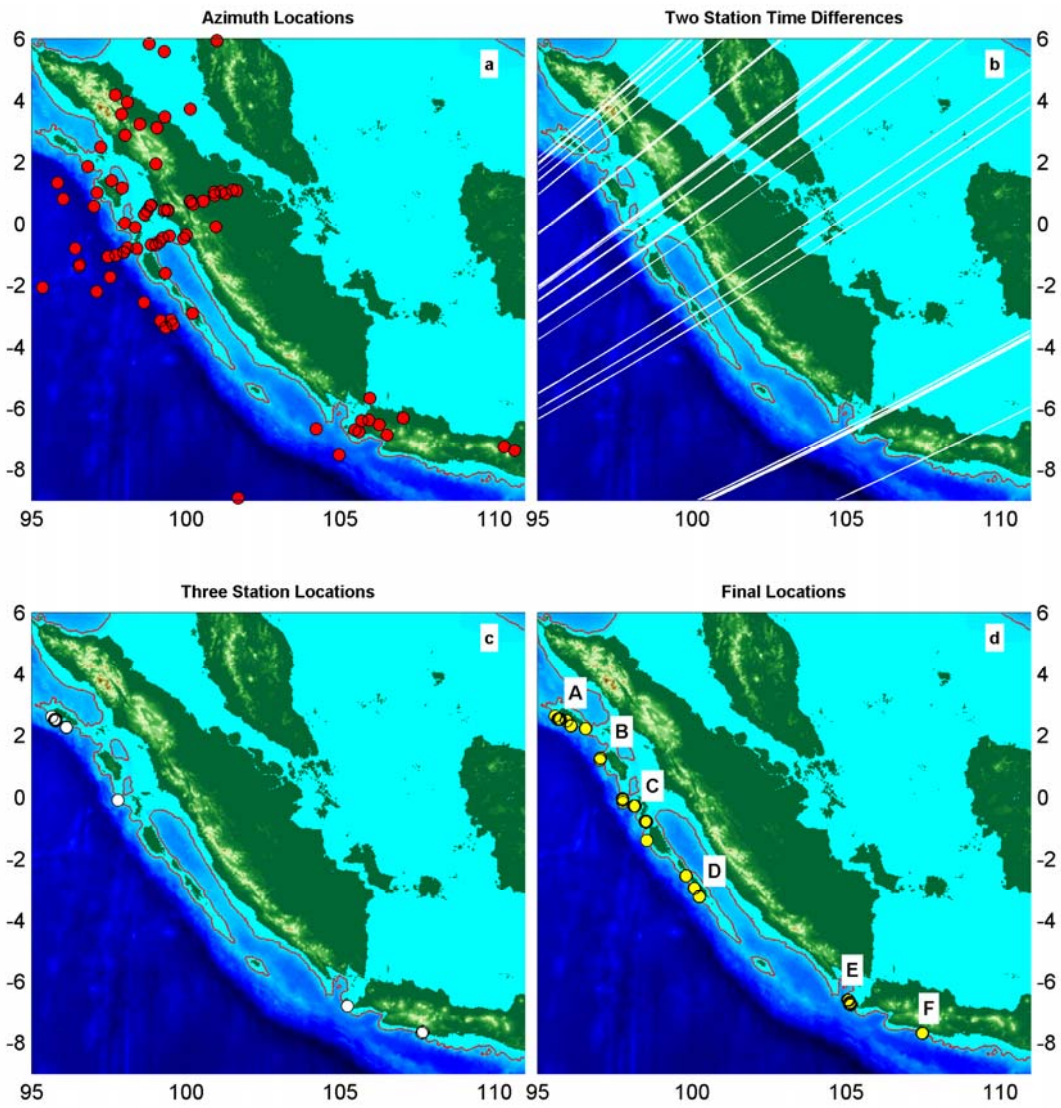

Figure 4. Location determination of 102 explosions west of Sumatra and Java. Seventy-nine explosions are observed at H08S and H04N, and 23 explosions are, in addition, observed at H01W. (a) Back-azimuth locations are consistent with Sumatra or Java sources, but with large uncertainty. (b) Constant arrival time difference curves for arrivals at H04N and H08S. (c) Three-station time-based locations for 23 explosions that lie along the western islands. (d) Locations based on location curves in (b) intersecting the 500 m bathymetry contour (red line).

The cepstral delays of the explosion arrivals are tightly clustered near 0.2 s at both H04N and H08S, suggesting that the explosions have similar sizes and depths. Bubble pulse estimates place a trade-off constraint on source size and depth. The bubble-pulse delay time estimates range from 0.1 to 0.5 s (Figure 5). The right panel of Figure 5 shows representative depth-yield tradeoff curves for cepstral delays from 0.10 to 0.25 s, which correspond to small or deep sources. Explosions with yields of 10 kg or less with a 0.2 s delay would have had to occur at depths less than 50 m.

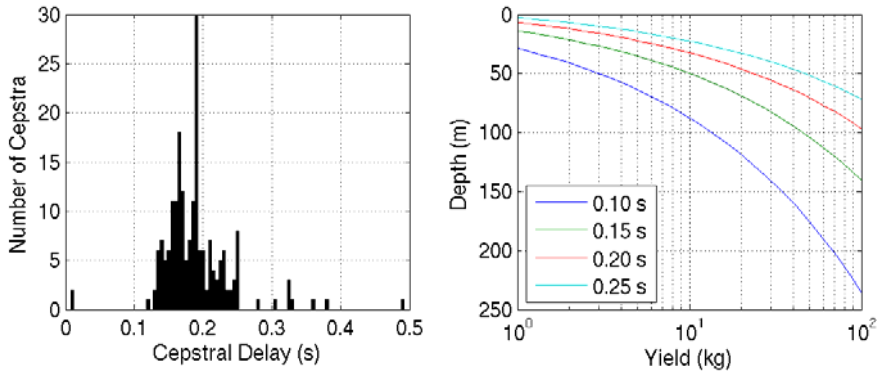

Figure 5. (a) Histogram of cepstral delays for all H01W, H04N and H08S arrivals associated to explosions offshore of Sumatra and Java. (b) Representative depth-yield tradeoff curves for selected cepstral delays.

The cepstral delay time values are useful in confirming the arrival associations. The cepstral delays estimate the bubble pulse periods of the explosions and, hence, should be independent of path and receiver effects. The mean difference in cepstral delay times estimated at H04N and H08S for 75 Sumatra and Java explosions is essentially zero with a standard deviation of less than 2 milliseconds. This is less than the sampling rate of the instruments (4 milliseconds between samples), which is possible because we interpolate the delay time.

The hypothesis that the Indonesian explosions are largely from blast fishing is somewhat surprising since we would expect these explosions to be small, shallow, and in shallow water, none of which are properties conducive to basin wide propagation. We conducted preliminary modeling to help determine how, or if, the signals from these explosions could make it into the sound channel. Figure 6 shows the sound speed profile for three depth ranges from the Generalized Digital Environmental Model (GDEM) offshore of equatorial Sumatra (blue line). The left panel shows the sound speed profile for the entire water column. The middle and right panels show the thermocline and mixed layer profiles, respectively. The red line is a simplified model for future sensitivity experiments that represents the surface duct as a single gradient defined by points at the surface and 75 meters, and the thermocline as a negative gradient defined by points at 100 and 200 meter depths. These two gradients are a good approximation to the GDEM data.

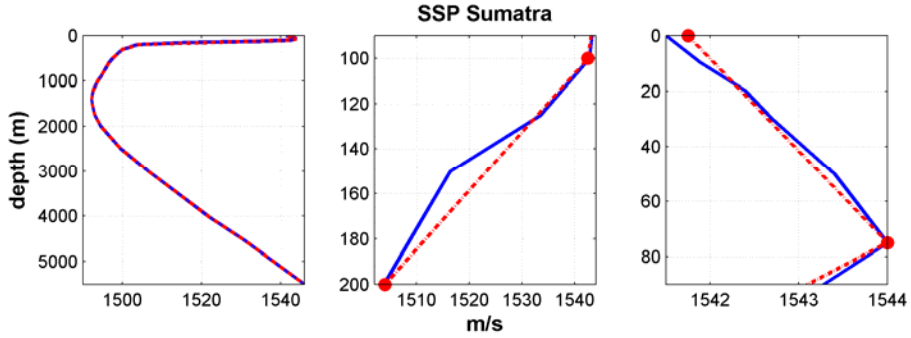

Figure 6. Sound speed profile from GDEM (blue) and simplified version (red) used in modeling hydroacoustic propagation in the equatorial Indian Ocean offshore of Sumatra.

We used the sound speed profile described above to model propagation with different source bathymetry to examine the possibility of getting energy from shallow explosions trapped and propagating horizontally in the sound channel. Figure 7 shows results from Gaussian beam ray tracing using BELLHOP (Porter and Bucker, 1987). The source frequency used for all models is 50 Hz, and the source depth is 25 meters. Rays were calculated for take-off angles ranging from -20 to +20 degrees. The first model (a) is for a range independent ocean (5,300 meters deep). It is clear that the sound bounces vertically with some energy trapped in the surface duct, but no energy is trapped in the deep sound channel. The next model (b) starts with a 6-degree wedge, which is a typical overall slope for the Sunda Trench. The wedge is effective at converting steep rays to horizontal rays, and then, because the ocean is deepening so quickly, the rays are trapped by the sound channel and do not interact with the seafloor. The third model (c) is the

same as (b) except the first 5 km is a 100-meter deep shelf. Energy still manages to enter the deep sound channel. The bottom model (d) uses an example of a more realistic trench bathymetry profile perpendicular to Sumatra (from ETOPO2). It is also effective at trapping energy into the deep sound channel. Bottom properties, including shear velocity, attenuation, and roughness, can diminish or enhance transmission into the sound channel, but it is clear that the bathymetry and sound speed profile near Sumatra conspire to allow small shallow explosions to be heard at basin-wide distances. Although shallow sources add complication to interpretation, they are probably more representative of realistic explosion monitoring type problems.

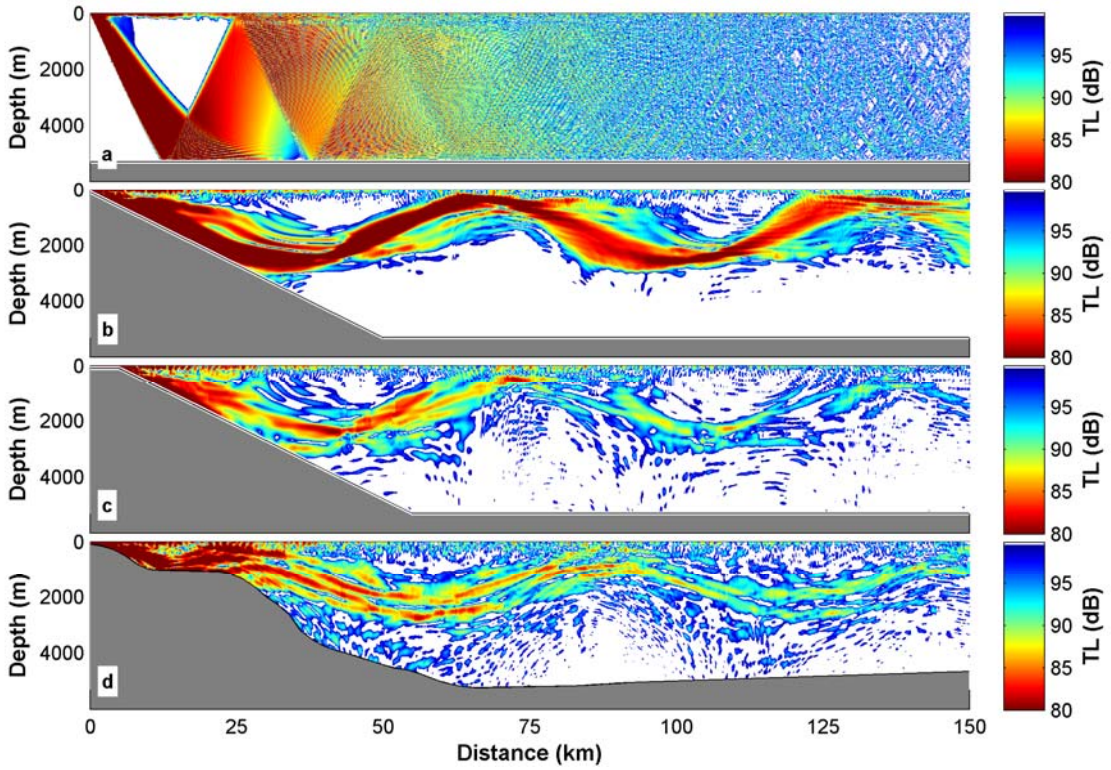

Figure 7. Transmission loss predicted from ray tracing for a source at 25 m depth and a frequency of 50 Hz for (a) open ocean, 5,300 m depth, (b) a 6º continental slope, (c) a 6º continental slope and a continental shelf 5 km wide, and (d) bathymetry from ETOPO2 (Smith and Sandwell, 1997).

Transmission Loss for Direct Arrivals

The explosions are located so that paths to different stations intersect different bathymetry. Most have direct deep water paths to at least one of the hydrophone triads. Attenuation estimates can be made by comparing amplitudes between stations. Explosions in Group A, near Simeulue Island, can be further divided into five sub-groups based on arrival time differences between H04N and H08S (Figure 4b). Figure 8 shows an example of observed variations in the relative received level for closely spaced events. Each panel shows the frequency dependent amplitude ratios between H04N and H08S relative to the expected loss based on distance traveled assuming cylindrical spreading and $0.5 \cdot 10^{-3}$ dB/km intrinsic attenuation (Urick, 1979). The explosions are separated by less than 100 km (small when compared to the 2,900 and 6,900 km paths to H08S and H04N, respectively). However, the relative amplitudes vary by more than 20 dB. Paths to both stations are generally deep and are rarely less than 2,000 m (except at the source). Conventional wisdom would expect little difference in attenuation among these paths. It is important to understand how these high frequency amplitude variations arise from such small differences in path.

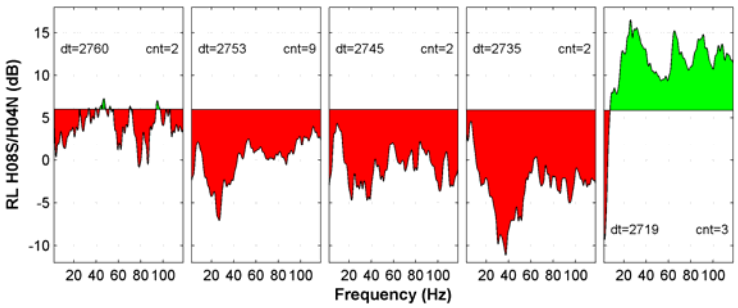

Figure 8. Frequency dependent received level (RL) differences between H08S and H04N for five slightly different paths in Group A. The arrival time differences (dt) and the number of events (cnt) are specified for each path. The water level is set to the expected RL difference assuming no obstacles (~6 dB). Red indicates that the signal is smaller than expected at H08S and green indicates that the signal is smaller than expected at H04N.

Paths from Group A explosions to H08S cross two potentially significant bathymetric features: The Ninety East Ridge and the Afanasiy-Nikitin Seamount (Box 1 and 2 in Figure 9). Paths to H04N only cross the Ninety East Ridge (Box 3). These sections of the Ninety East Ridge are relatively deep. The Afanasiy-Nikitin Seamount rises up to 1,800 m below sea level. Although this is deeper than the sound channel axis, it is still a significant impediment to sound propagation. The section of the Ninety East Ridge that these paths intersect is likely too deep to have much effect on transmission.

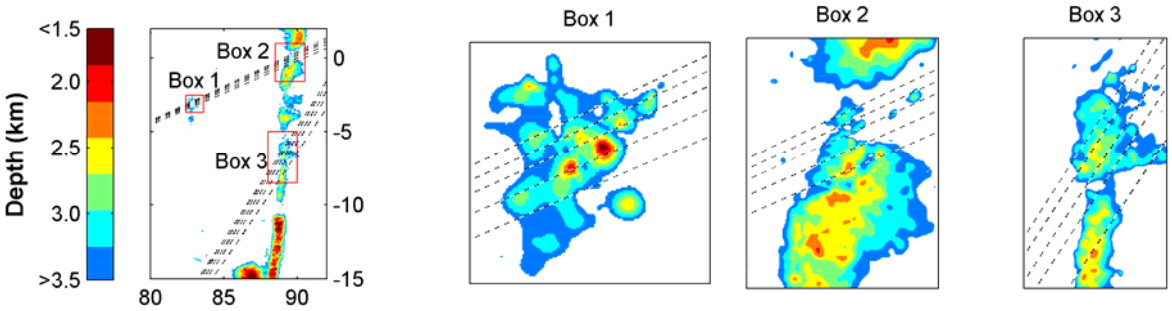

Figure 9. Significant bathymetry along Group A explosions paths to H08S (northern dashed lines) and H04N (southern dashed lines). The five paths are for the clusters within Group A (Figure 4)—the northern most path corresponds to the left most panel in Figure 8. Paths to H08S intersect the Afanasiy-Nikitin Seamount (Box 1) and the Ninety East Ridge (Box 2). Paths to H04N also intersect the Ninety East Ridge (Box 3). The bathymetry is from ETOPO2.

Modeling hydroacoustic transmission loss (TL) can be a difficult problem. Although there has been much success with TL modeling provided enough environmental constraints, general basin-wide TL modeling is not yet practical. Not only do global databases lack the necessary resolution in bathymetry and accuracy in seafloor properties, but also unknowns in source factors make highly precise, and not necessarily accurate, modeling of dubious value. We are taking a more statistical approach to the problem that if properly calibrated should be of use for understanding the uncertainties in hydroacoustic monitoring capabilities. At the distances and frequencies of most interest to nuclear-test monitoring (2 to 100 Hz) intrinsic attenuation is small, and most attenuation other than geometrical spreading is caused by interaction with the seafloor or sea-surface. The sound that propagates thousands of kilometers will consist of a narrow set of rays. The angles of the ray bundle as measured at the sound channel axis will generally be less than 10 degrees. Assuming the rays have constant horizontal slowness, the grazing angle at the seafloor will be less than 10 degrees, which is generally less than the critical grazing angle for typical compressional velocities. Thus, reflection loss will be due to intrinsic P-wave attenuation or due to the seafloor supporting shear waves.

Our approach is to approximate the seafloor interaction at any given point as a function of ray angle measured at the sound channel axis. Using a ray theoretical model, we define the signal loss per distance traveled as a function of ray parameter, p, for a given sound speed profile, $v(z)$, and sea bottom depth, z_b, as

$$\chi(p : v(z), z_b) = N(p) \cdot BL(\theta(p : z = z_b)) \text{ where } BL = -10 \cdot \log(R(\theta)) \qquad (1)$$

N is the number of ray interactions per distance traveled, and R is the reflection coefficient as a function of grazing angle, θ. We assume that the bottom loss is proportional to the vertical slowness, which at small angles is proportional to the grazing angle. The number of ray interactions per distance traveled can be calculated from the eikonal equation assuming constant ray parameter and integrating along path (e.g., Lay and Wallace, 1995):

$$N(p) = \left[2p \int_{z_b}^{z_0} \left[\gamma^2 + p^2 \right]^{-1/2} dz \right]^{-1} \tag{2}$$

where z_0 is the ray's turning point, and γ is slowness as a function of depth. We are most interested in estimating a reasonable variance on the signal loss along the path. We use the sensitivity of our modeled signal loss to grazing angle at the seafloor as a measure of uncertainty by assuming that the attenuation per reflection is proportional to the grazing angle. For shallow grazing angles (which rays at long distance must be), this is a reasonable first approximation. By taking partial derivatives with respect to the grazing angle at the seafloor, a variance in bottom loss with distance can be estimated:

$$\mathrm{var}(BL) = \alpha^2 \left(\frac{\partial N}{\partial \theta} \theta + N \right)^2 \delta\theta^2 \tag{3}$$

Figure 10 shows the function of seafloor interaction versus depth and take-off angle for two sound speed profiles. The first sound speed profile is the Munk Profile (1974), and the second is an equatorial Indian Ocean profile extracted from GDEM. The area in white indicates zero interaction (rays turn before hitting bottom), and the areas in red indicate strong seafloor interaction. The Indian Ocean sound speed profile has a broader sound channel as indicated by the width of blue in the figure. The ray interaction for a 2,500-meter deep seafloor in the equatorial Indian Ocean only begins for angles greater than 6 degrees, but a 1,750-meter deep seafloor has ray interaction starting at 2 degrees. This may seem like a small difference, but it is a large proportion of a ray packet that travels long distance.

In the case of shallow explosions, like those west of Indonesia, steeper ray angles between 2 and 6 degrees are critical, as can be seen from the ray tracing results in Figure 7. This helps explain the strong sensitivity of received levels to slight variations in the paths crossing the Afanasiy-Nikitin Seamount observed in Figure 8. If the seamount were in an area with a more typical sound speed profile, such as found at higher latitudes, it would probably cause little attenuation of the signal.

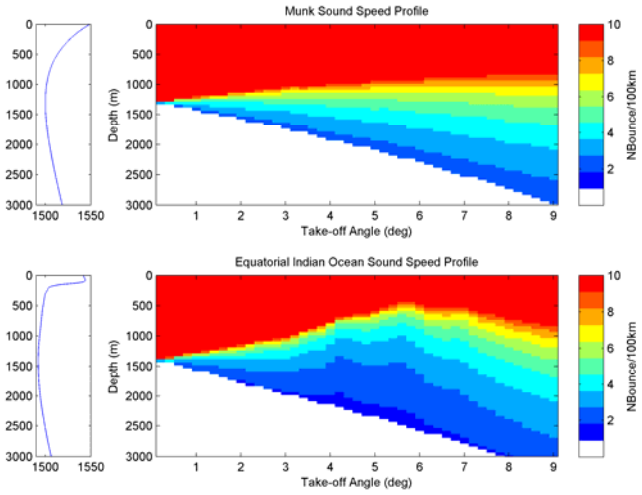

Figure 10. Contour plot of the number of bounces per 100 km as a function of take-off angle and water depth for (upper panel) the Munk (1974) sound speed profile (shown to left), and (lower panel) a GDEM profile for the equatorial Indian Ocean. The sound speed profile for the Indian Ocean increases the maximum bathymetric depth predicted to interact with explosion signals.

CONCLUSION AND RECOMMENDATION

We developed a discovery procedure that searches automatic processing results for explosion-like signals. From this procedure, we identified 305 previously unknown explosions located in three general areas of the Indian Ocean. The explosion signals are broadband and often contain reflected signals. We have shown that small shallow explosions can, given the right source geometry, propagate signals to basin-wide distances. Many of the direct arrivals are observed at multiple stations, which we have used to determine precise locations. The observed attenuation can be very sensitive to slight variations in bathymetry, which is probably enhanced due to the sound speed profiles of the equatorial Indian Ocean and the shallow nature of the sources.

ACKNOWLEDGEMENTS

We thank Manocher Bahavar and Paul Piraino for obtaining the hydrophone data used in this research.

REFERENCES

Blackman, D. K., J. A. Mercer, R. Andrew, C D. de Groot-Hedlin, and P. E. Harben (2003). Indian Ocean calibration tests: Cape Town-Cocos Keeling 2003, in *Proceedings of the 25th Seismic Research Review—Nuclear Explosion Monitoring: Building the Knowledge Base,* LA-UR-03-6029, Vol. 1, pp. 517–523.

Bowman, J. R., J. A. Hanson, and D. Jepsen (2005). An active-source experiment in the Indian Ocean, in *Proceedings of the 27th Seismic Research Review: Ground-Based Nuclear Explosion Monitoring Technologies*, LA-UR-05-6407, Vol. 2, pp. 722–732.

Brumbaugh, D. A. and R. J. Le Bras (1998). Hydroacoustic signals from a ground-truth data set of marine explosions, SAIC technical report, SAIC-98/3008.

Graeber, F. and P. Firbas (2005). Recent developments in hydroacoustic data processing at the IDC, *Hydroacoustic Workshop*, Victoria, British Columbia, May 1–5.

Hanson, J. A. and J. R. Bowman (2006). Methods for monitoring hydroacoustic events using direct and reflected T waves in the Indian Ocean, *J. Geophys. Res*. doi:10.1029/2004JB003609.

Hanson, J. A., C. L. Reasoner, and J. R. Bowman (2007). Investigations of natural events in the Indian Ocean using three hydrophone stations, SAIC Technical Report SAIC-07/3019.

Hanson, J., R. Le Bras, P. Dysart, D. Brumbaugh, A. Gault, and J. Guern (2001). Operational processing and special studies of hydroacoustics at the Prototype International Data Center, *Pure and Applied Geophysics*, 158 425–456.

Lay, T. and T. C. Wallace (1995). *Modern Global Seismology*, Academic Press, p78.

Munk, W.H. (1974). Sound channel in an exponentially stratified ocean with applications to SOFAR, *J. Acoust. Soc. Am.* 55: 220–226.

Porter, M. B. and H. P. Bucker (1987). Gaussian beam tracing for computing ocean acoustic fields, *J. Acoust. Soc. Amer.* 82: 1349–1359.

Reasoner, C.L., J.A. Hanson. and J. R. Bowman (2005). Characterization of two underwater explosions in the Bay of Bengal on May 5, 2004, SAIC Technical Report SAIC-05/3001.

Smith, W. H. F., and D. T. Sandwell, (1997). Global seafloor topography from satellite altimetry and ship depth soundings, *Science* 277: 1957–1962.

Spiliopoulos, S. and D. Jepsen (2005). Studies in the Indian Ocean: Preliminary phase identification and synergies with the seismic network, *Hydroacoustic Workshop*, Victoria, BC, May 1–5, 2005.

Urick, R.J. (1979). *Sound Propagation in the Sea*, Defense Advanced Research Projects Agency, Washington, D.C.